Title	Assumed strain and hybrid destabilized ten-node C degree triangular shell elements
Author(s)	Sze, KY; Zhu, D
Citation	Computational Mechanics, 1998, v. 21 n. 2, p. 161-171
Issued Date	1998
URL	http://hdl.handle.net/10722/54317
Rights	Creative Commons: Attribution 3.0 Hong Kong License

Assumed Strain and Hybrid Destabilized Ten-node C^0 Triangular Shell Elements

K.Y.Sze , Dan Zhu*
Department of Mechanical Engineering, The University of Hong Kong
Pokfulam Road, HONG KONG

ABSTRACT

The conventional ten-node C^0 triangular shell element is in general too stiff. In this paper, several less stiff formulations are proposed. To reduce the transverse shear stiffness, the assumed strain method is adopted. On the other hand, both assumed strain method and hybrid destabilization are employed for softening the membrane stiffness. The improvement is validated by popular numerical problems.

keywords : triangular, shell, finite element, assumed strain, hybrid destabilization, Mindlin/Reissner

* on leave from *Southwest Jiaotong University, Chengdu, Sichuan 610031, P.R.CHINA*

Published in Computational Mechanics 21 (1998) 161- 171

1. INTRODUCTION

As motivated by the need of advanced triangular elements for automatic mesh generation and refinement, quadratic and cubic C^0 plate bending elements have been developed recently by Sze, Zhu & Chen (1997) and Sze & Zhu (1997a). These elements are developed by observing the following criteria : (a) their kinematics has not been modified by the Kirchhoff constraints such that they are applicable for thick and laminated plate/shell analyses in addition to thin plate/shell analyses, (b) they possess no commutable spurious zero energy modes, (c) they do not exhibit shear locking, (d) they pass the constant moment and constant shear patch tests, (e) their boundary nodes have the same number of d.o.f.s so that they present no complication for being implemented in any finite element code. In this paper, "shear" refers to "transverse shear" unless otherwise specified. Moreover, a quadratic curved shell element has also been developed by including the requirements of (f) satisfying the 2/D membrane patch test and (g) being free from membrane locking (Sze & Zhu 1997b).

Same as the conventional or displacement-based quadratic triangular C^0 shell element, the cubic one is in general too stiff. It is also noted that there are only very few articles devoted to its improvement. Among them, Lee et al. (1985) proposed two ten-node hybrid strain elements. The first element contains nine assumed membrane strain modes and six assumed shear strain modes whereas the second element contains eighteen assumed membrane strain modes and twelve assumed shear strain modes. The first element does not suffer from shear lockings but exhibits twelve spurious zero energy modes. On the other hand, the second element suffers from lockings but does not exhibit any spurious zero energy modes. A quadrilateral macro-element composed of two elements of each kind was formed. It happens that the macro-element does not suffer from lockings and spurious zero energy modes. Unfortunately, it does not possess the advantage of triangular elements in automatic mesh generation and refinement.

A cubic plate bending triangular element is the assumed strain MITC12 element (Bathe et al. 1990; Bathe 1996). It contains nine boundary nodes and four bubble nodes. Three bubble nodes are equipped with rotational d.o.f.s only whereas the remaining one is equipped with translational d.o.f. only. The shear strain field is constructed from fifteen shear strain samples out of which nine are tangential to the element edges. It appears to us that MITC12 is the only cubic element that fulfills criteria (a) to (e). Nevertheless, MITC12 is expensive due to the presence of the four bubble nodes and the required thirteen-point integration rule. To our best knowledge, shell counterpart of MITC12 does not exist.

Very recently, Sze & Zhu (1997a) have derived the assumed strain AST10O plate bending element. The element matrix is computed by the six-point rule (Cook et al. 1989) and six out of its twelve shear strain samples are shifted from the integration stations to the element edges. The constraint ratio of the element is then increased from 1.125 to 1.5 which is the optimal value suggested by Hughes (1987). AST10O yields more accurate results than its displacement counterpart. In this paper, AST10O will be generalized to curved shell analyses. To alleviate the excessive membrane stiffness in the element, two methods are employed. One is the assumed

natural strain formulation in which the three natural membrane normal strains are interpolated independently at their sampling points which are different from the integration stations. The other method is the hybrid destabilization (Sze 1993; Sze et al. 1995). The latter induces two incommutable spurious zero energy modes to the element so as to reduce the number of membrane constraints. Popular numerical tests are exercised. The proposed methods are found to be efficacious.

2. FORMULATION OF THE CONVENTIONAL TEN-NODE C^0 SHELL ELEMENT

This section describes the geometry and kinematic of the conventional ten-node shell based on the degenerated solid approach (e.g., see Ahmad et al. 1970; Zienkiewicz & Taylor 1989; Sze 1994; Brank, Peric & Damjanic 1995; Basar & Ding 1996; Sze, Sim & Soh 1997).

2.1 Global Cartesian Coordinates and Natural Coordinates Fig.1 shows a ten-node curved shell element. Global Cartesian coordinates (*X*,*Y*,*Z*) of any point along the *i*-th nodal normal of the element can be expressed as :

$$\mathbf{X}_i = \mathbf{X}_{oi} + \zeta \mathbf{X}_{ni} \tag{1a}$$

where $\zeta \in [-1,+1]$ is the transverse natural coordinate, $\mathbf{X}_{oi}$ is the position vector of the node and $\mathbf{X}_{ni}$ is the nodal normal vector. It can be noted that $\|\mathbf{X}_{ni}\|$, the magnitude of $\mathbf{X}_{ni}$, equals half of the nodal thickness h_i. The mapping between the global Cartesian coordinates (*X*,*Y*,*Z*) and the parametric coordinates (s,t,ζ), see Fig.2a, is set up by the standard interpolation :

$$\mathbf{X}(s,t,\zeta) = \sum_{i=1}^{10} N_i(s,t)\mathbf{X}_i = \mathbf{X}_o(s,t) + \zeta \mathbf{X}_n(s,t) \tag{1b}$$

where

$$\mathbf{X}_o = \sum_{i=1}^{10} N_i(s,t)\mathbf{X}_{oi} \ , \ \mathbf{X}_n = \sum_{i=1}^{10} N_i(s,t)\mathbf{X}_{ni} \ , \ N_1 = (3r-1)(3r-2)r/2$$

$$N_2 = 9rs(3r-1)/2 \ , \ N_3 = 9rs(3s-1)/2 \ , \ N_4 = (3s-1)(3s-2)s/2$$

$$N_5 = 9st(3s-1)/2 \ , \ N_6 = 9st(3t-1)/2 \ , \ N_7 = (3t-1)(3t-2)t/2$$

$$N_8 = 9tr(3t-1)/2 \ , \ N_9 = 9tr(3r-1)/2 \ , \ N_{10} = 27rst \ , \ r = 1 - s - t$$

In the above expressions, r is also an area coordinate but treated as one dependent on s and t in this section.

2.2 Description of Element Kinematics At each node, two vectors both perpendicular to the nodal normal and of magnitude equal to half of the nodal thickness are defined :

$$\mathbf{f}_i^1 = \begin{cases} \dfrac{h_i}{2}\dfrac{\mathbf{X}_{ni}\times\mathbf{e}_Z}{\left\|\mathbf{X}_{ni}\times\mathbf{e}_Z\right\|} = \dfrac{h_i}{2}\dfrac{[Y_{ni},-X_{ni},0]^T}{\sqrt{X_{ni}^2+Y_{ni}^2}} & \text{for} \quad X_{ni}^2+Y_{ni}^2 \neq 0 \\ \dfrac{h_i}{2}[1,0,0]^T & \text{for} \quad X_{ni}^2+Y_{ni}^2 = 0 \end{cases} \tag{2a}$$

$$\mathbf{f}_i^2 = \frac{2}{h_i}(\mathbf{X}_{ni}\times\mathbf{f}_i^1) \tag{2b}$$

where $\mathbf{e}_Z = [0,0,1]^T$ is the unit vector in the Z-direction. Besides the three nodal translations U_{oi}, V_{oi} and W_{oi}, there are also two nodal rotations θ_i^1 and θ_i^2 which are respectively the rotations about $\mathbf{f}_i^1$ and $\mathbf{f}_i^2$, see Fig.1. Thus, the displacement at any point along the i-th nodal normal is :

$$\mathbf{U}_i = \mathbf{U}_{oi} + \zeta\mathbf{U}_{ni} \tag{3a}$$

in which

$$\mathbf{U}_o = \begin{bmatrix} U_o & V_o & W_o \end{bmatrix}^T \ , \ \mathbf{U}_{oi} = \begin{bmatrix} U_{oi} & V_{oi} & W_{oi} \end{bmatrix}^T \ , \ \mathbf{U}_{ni} = \begin{bmatrix} -\mathbf{f}_i^2 & \mathbf{f}_i^1 \end{bmatrix} \begin{Bmatrix} \theta_i^1 \\ \theta_i^2 \end{Bmatrix}$$

Similar to the coordinates, the interpolated displacement is :

$$\mathbf{U}(s,t,\zeta) = \sum_{i=1}^{10} N_i(s,t)\mathbf{U}_i = \mathbf{U}_o(s,t) + \zeta\mathbf{U}_n(s,t) \tag{3b}$$

where

$$\mathbf{U}_o = \mathbf{U}_o(s,t) = \sum_{i=1}^{10} N_i(s,t)\mathbf{U}_{oi} = \begin{bmatrix} N_1\mathbf{I}_3, \mathbf{0}_{3\times 2}, \ldots, N_{10}\mathbf{I}_3, \mathbf{0}_{3\times 2} \end{bmatrix}\mathbf{q}$$

$$\mathbf{U}_n = \mathbf{U}_n(s,t) = \sum_{i=1}^{10} N_i(s,t)\mathbf{U}_{ni} = [\mathbf{0}_{3\times 3}, -\mathbf{f}_1^2 N_1, \mathbf{f}_1^1 N_1, \ldots, \mathbf{0}_{3\times 3}, -\mathbf{f}_{10}^2 N_{10}, \mathbf{f}_{10}^1 N_{10}]\mathbf{q}$$

$\mathbf{q} = [U_1, V_1, W_1, \theta_1^1, \theta_1^2, \ldots, U_{10}, V_{10}, W_{10}, \theta_{10}^1, \theta_{10}^2]^T$ is the element displacement vector

2.3 Natural Strains The inplane and transverse shear natural strains defined with respect to the *s-t-*ζ-coordinates are (e.g., see Fung 1965; Sze 1994; Sze, Sim & Soh 1997) :

$$\varepsilon_{ss} = \mathbf{X}_{,s}^T\mathbf{U}_{,s} \ , \ \varepsilon_{tt} = \mathbf{X}_{,t}^T\mathbf{U}_{,t} \ , \ 2\varepsilon_{st} = \mathbf{X}_{,s}^T\mathbf{U}_{,t} + \mathbf{X}_{,t}^T\mathbf{U}_{,s} \tag{4a}$$

$$\gamma_{\zeta s} = \mathbf{X}_{,\zeta}^T\mathbf{U}_{,s} + \mathbf{X}_{,s}^T\mathbf{U}_{,\zeta} \ , \ \gamma_{\zeta t} = \mathbf{X}_{,\zeta}^T\mathbf{U}_{,t} + \mathbf{X}_{,t}^T\mathbf{U}_{,\zeta} \tag{4b}$$

By retaining up to the first order ζ-terms in the inplane strains (ε_{ss}, ε_{tt} and $2\varepsilon_{st}$) and the zeroth order ζ-terms in the transverse shear strains ($\gamma_{\zeta s}$ and $\gamma_{\zeta t}$), we have

$$\varepsilon_{ss} = \varepsilon_{ss}^m + \zeta\varepsilon_{ss}^b \ , \ \varepsilon_{tt} = \varepsilon_{tt}^m + \zeta\varepsilon_{tt}^b \ , \ 2\varepsilon_{st} = 2\varepsilon_{st}^m + 2\zeta\varepsilon_{st}^b \tag{5a}$$

$$\gamma_{\zeta s} = \mathbf{X}_n^T\mathbf{U}_{o,s} + \mathbf{X}_{o,s}^T\mathbf{U}_n \ , \ \gamma_{\zeta t} = \mathbf{X}_n^T\mathbf{U}_{o,t} + \mathbf{X}_{o,t}^T\mathbf{U}_n \tag{5b}$$

where

$$\varepsilon_{ss}^{m} = \mathbf{X}_{o,s}^{T}\mathbf{U}_{o,s} \ , \ \varepsilon_{tt}^{m} = \mathbf{X}_{o,t}^{T}\mathbf{U}_{o,t} \ , \ 2\varepsilon_{st}^{m} = \mathbf{X}_{o,s}^{T}\mathbf{U}_{o,t} + \mathbf{X}_{o,t}^{T}\mathbf{U}_{o,s} \ , \ \varepsilon_{ss}^{b} = \mathbf{X}_{n,s}^{T}\mathbf{U}_{o,s} + \mathbf{X}_{o,s}^{T}\mathbf{U}_{n,s}$$
$$\varepsilon_{tt}^{b} = \mathbf{X}_{n,t}^{T}\mathbf{U}_{o,t} + \mathbf{X}_{o,t}^{T}\mathbf{U}_{n,t} \ , \ 2\varepsilon_{st}^{b} = \mathbf{X}_{n,s}^{T}\mathbf{U}_{o,t} + \mathbf{X}_{n,t}^{T}\mathbf{U}_{o,s} + \mathbf{X}_{o,s}^{T}\mathbf{U}_{n,t} + \mathbf{X}_{o,t}^{T}\mathbf{U}_{n,s}$$

In the above expressions, "*m*" and "*b*" abbreviate "membrane" and "bending", respectively.

2.4 Local Cartesian Coordinates Material properties are often specified or defined with respect to a local Cartesian coordinate system whose x-y-plane is tangential to the mid-surface. At any point on the mid-surface, the unit vectors along the axes of any local Cartesian system (x,y,z) can be expressed by :

$$\mathbf{e}_z = \frac{\mathbf{X}_{o,s} \times \mathbf{X}_{o,t}}{\left\| \mathbf{X}_{o,s} \times \mathbf{X}_{o,t} \right\|} \ , \ \mathbf{e}_x = \frac{\mathbf{v}_{ref} \times \mathbf{e}_z}{\left\| \mathbf{v}_{ref} \times \mathbf{e}_z \right\|} \ , \ \mathbf{e}_y = \mathbf{e}_z \times \mathbf{e}_x \tag{6}$$

where the reference vector $\mathbf{v}_{ref}$ is most conveniently taken to be an inplane principal material direction. For isotropic materials, $\mathbf{v}_{ref} = \mathbf{X}_{o4} - \mathbf{X}_{o1}$ is assumed for simplicity. As $\mathbf{X}_n$ is parallel or approximately parallel to $\mathbf{e}_z$, we have

$$\left[\begin{matrix} x_{,s} & x_{,t} & x_{,\zeta} \\ y_{,s} & y_{,t} & y_{,\zeta} \\ z_{,s} & z_{,t} & z_{,\zeta} \end{matrix} \right]_{\zeta=0} = \left[\begin{matrix} \mathbf{e}_x^T \\ \mathbf{e}_y^T \\ \mathbf{e}_z^T \end{matrix} \right] \left[\mathbf{X}_{o,s} \quad \mathbf{X}_{o,t} \quad \mathbf{X}_n \right] \cong \left[\begin{matrix} \mathbf{e}_x^T\mathbf{X}_{o,s} & \mathbf{e}_x^T\mathbf{X}_{o,t} & 0 \\ \mathbf{e}_y^T\mathbf{X}_{o,s} & \mathbf{e}_y^T\mathbf{X}_{o,t} & 0 \\ 0 & 0 & \mathbf{e}_z^T\mathbf{X}_n \end{matrix} \right] \tag{7}$$

Owing to the approximate vanishing nature of $x_{,\zeta}$, $y_{,\zeta}$, $z_{,s}$ and $z_{,t}$, the local Cartesian strain can be obtained via tensor transformation as :

$$\boldsymbol{\varepsilon}^m = \left\{ \begin{matrix} \varepsilon_{xx}^m \\ \varepsilon_{yy}^m \\ 2\varepsilon_{xy}^m \end{matrix} \right\} = \mathbf{T}_\varepsilon \left\{ \begin{matrix} \varepsilon_{ss}^m \\ \varepsilon_{tt}^m \\ 2\varepsilon_{st}^m \end{matrix} \right\} \ , \ \boldsymbol{\varepsilon}^b = \left\{ \begin{matrix} \varepsilon_{xx}^b \\ \varepsilon_{yy}^b \\ 2\varepsilon_{xy}^b \end{matrix} \right\} = \mathbf{T}_\varepsilon \left\{ \begin{matrix} \varepsilon_{ss}^b \\ \varepsilon_{tt}^b \\ 2\varepsilon_{st}^b \end{matrix} \right\} \ , \ \boldsymbol{\gamma} = \left\{ \begin{matrix} \gamma_{\zeta s} \\ \gamma_{\zeta t} \end{matrix} \right\} = \mathbf{T}_\gamma \left\{ \begin{matrix} \gamma_{\zeta s} \\ \gamma_{\zeta t} \end{matrix} \right\} \tag{8}$$

where

$$\mathbf{T}_\varepsilon = \left[\begin{matrix} x_{,s}\, x_{,s} & y_{,s}\, y_{,s} & x_{,s}\, y_{,s} \\ x_{,t}\, x_{,t} & y_{,t}\, y_{,t} & x_{,t}\, y_{,t} \\ 2x_{,s}\, x_{,t} & 2y_{,s}\, y_{,t} & x_{,s}\, y_{,t} + x_{,t}\, y_{,s} \end{matrix} \right]_{\zeta=0}^{-1} \ , \ \mathbf{T}_\gamma = \left[\begin{matrix} z_{,\zeta}\, x_{,s} & z_{,\zeta}\, y_{,s} \\ z_{,\zeta}\, x_{,t} & z_{,\zeta}\, y_{,t} \end{matrix} \right]_{\zeta=0}^{-1}$$

By consolidating Eqn.(1b), Eqn.(3b), Eqn.(5) and Eqn.(8), the local Cartesian strains can be expressed in terms of the element displacement vector. Symbolically,

$$\boldsymbol{\varepsilon}_m = \mathbf{B}_m\mathbf{q} \ , \ \boldsymbol{\varepsilon}_b = \mathbf{B}_b\mathbf{q} \ , \ \boldsymbol{\gamma} = \mathbf{B}_\gamma\mathbf{q} \tag{9}$$

To compute the element stiffness matrix, the potential energy functional is employed :

$$\Pi_P^e = \int_{-1}^{+1}\int_0^1\int_0^{1-t}\left((\boldsymbol{\varepsilon}_m+\zeta\,\boldsymbol{\varepsilon}_b)^T\mathbf{C}_\varepsilon(\boldsymbol{\varepsilon}_m+\zeta\,\boldsymbol{\varepsilon}_b)+\boldsymbol{\gamma}^T\mathbf{C}_\gamma\,\boldsymbol{\gamma}\right)J\,ds\,dt\,d\zeta \tag{10}$$

in which J is the Jacobian determinant for the transformation from (X,Y,Z) to (s,t,ζ), $\mathbf{C}_\varepsilon$ and $\mathbf{C}_\gamma$ are the inplane plane stress and transverse shear material stiffness matrices, respectively. The load term is ignored for simplicity. In case of isotropic materials,

$$\mathbf{C}_\varepsilon = \frac{E}{(1-\nu^2)}\begin{bmatrix}1 & \nu & 0\\ \nu & 1 & 0\\ 0 & 0 & (1-\nu)/2\end{bmatrix}\ ,\ \mathbf{C}_\gamma = \frac{kE}{2(1+\nu)}\begin{bmatrix}1 & 0\\ 0 & 1\end{bmatrix} \tag{11}$$

where E is elastic modulus, ν is the Poisson's ratio and k is the shear correction factor commonly taken as 5/6. By adopting the conventional approximation of $J \approx J(\zeta=0)$ and assuming the material matrices being independent of ζ, the functional can be simplified as :

$$\Pi_P^e = 2\int_0^1\int_0^{1-t}(\boldsymbol{\varepsilon}_m^T\mathbf{C}_\varepsilon\,\boldsymbol{\varepsilon}_m+\zeta^2\,\boldsymbol{\varepsilon}_b^T\mathbf{C}_\varepsilon\,\boldsymbol{\varepsilon}_b+\boldsymbol{\gamma}^T\mathbf{C}_\gamma\,\boldsymbol{\gamma})\,J(\zeta=0)\,ds\,dt \tag{12}$$

It should be remarked that the material matrices are functions of ζ for composite laminates. Thus, the bending and membrane energies may be coupled.

Based on the above Π_P^e and the six-point integration rule which is sufficient to secure the proper element rank, the element stiffness matrix is :

$$\mathbf{k} = \mathbf{k}_m + \mathbf{k}_b + \mathbf{k}_\gamma \tag{13}$$

where

$\mathbf{k}_m = 2\sum_{i=a}^{f}\mathbf{B}_{mi}^T\mathbf{C}_\varepsilon\mathbf{B}_{mi}w_iJ_i(\zeta=0)$, $\mathbf{k}_b = \frac{2}{3}\sum_{i=a}^{f}\mathbf{B}_{bi}^T\mathbf{C}_\varepsilon\mathbf{B}_{bi}w_iJ_i(\zeta=0)$

$\mathbf{k}_\gamma = 2\sum_{i=a}^{f}\mathbf{B}_{\gamma i}^T\mathbf{C}_\gamma\mathbf{B}_{\gamma i}w_iJ_i(\zeta=0)$, w_i's are the weighting factors of the integration rule

i is the designation for the integration station

The (r,s,t) values of the integration stations a, b and c are permutations of α, α and 1- 2α where $\alpha \approx$ 0.445948. On the other hand, (r,s,t) values of the integration stations d, e and f are permutations of β, β and 1-2β where $\beta \approx 0.091576$ (Cook et al. 1989), see Fig.2a.

3. ASSUMED SHEAR STRAINS

Generally speaking, assumed strain method overcomes shear/membrane locking by sampling strain components which are tangential to the element edges. Interested readers can find a comprehensive review on assumed strain method in the paper by Militello & Felippa (1991). Following the terminology of Saleeb et al (1988), these strains are here referred to as edge strains. Every of the sampled shear/membrane strains becomes a numerical penalty constraints when the thickness is small. It happens that the two edge strains sampled by adjacent elements at the same boundary point are identical and they constitute only one shear/membrane constraint. Consequently, the number of constraints in the global level are reduced (e.g., see Hughes 1987; Saleeb et al 1988; Zienkiewicz & Taylor 1989; Cook et al.1989). Same as other finite element techniques, assumed strain method is not foolproof. In order that an element is rank sufficient, a sufficient number of strains must be sampled. If the number of sampled strains is excessive, locking cannot be circumvented. On the other hands, a cyclic symmetric sampling pattern must be adopted or the element will be sensitive to different node numbering schemes and/or frame variant. These perhaps explains why, to our best knowledge, there exists no assumed strain curved C^0 shell triangles except for those devised very recently by Flores, Oñate & Zarate (1996) and Sze & Zhu (1997b).

In this paper, the assumed shear strain field is constructed analogous to that of our AST10O plate bending element (Sze & Zhu 1997a). Edge natural shear strains are sampled, see Fig.2b, which are :

$$\widehat{\gamma}_{\zeta r}(r) = \left(\mathbf{X}_n^T(\partial_r \mathbf{U}_0) + (\partial_r \mathbf{X}_0^T)\mathbf{U}_n\right)\Big|_{s=0} \ , \ \widehat{\gamma}_{\zeta s}(s) = \left(\mathbf{X}_n^T(\partial_s \mathbf{U}_0) + (\partial_s \mathbf{X}_0^T)\mathbf{U}_n\right)\Big|_{t=0} \ ,$$
$$\widehat{\gamma}_{\zeta t}(t) = \left(\mathbf{X}_n^T(\partial_t \mathbf{U}_0) + (\partial_t \mathbf{X}_0^T)\mathbf{U}_n\right)\Big|_{r=0} \qquad (14)$$

The differential operators ∂_r, ∂_s and ∂_t when operate on a function $F = F(r, s, t)$ are defined as :

$$\partial_r F(r,s,t) = \frac{\partial}{\partial r} F(r,s,1-r-s) \ , \ \partial_s F(r,s,t) = \frac{\partial}{\partial s} F(1-s-t,s,t) \ ,$$
$$\partial_t F(r,s,t) = \frac{\partial}{\partial t} F(r,1-t-r,t) \qquad (15)$$

It is noted that when the nodal d.o.f.s of a subparametric element are prescribed according to a third order pure moment field, the edge shear strains do not vanish in general. However, there are nine exceptional points which locate at 1/2 - √5/6, 1/2, 1/2 + √5/6 of the area coordinates. In other words, there are three optimal edge shear strains per edge. On the other hand, the postulated optimal constraint ratio (Hughes 1987) which equals to 3/2 for C^0 plate bending element can be achieved by sampling six edge and six non-edge shear constraints. Following our previous technique, the three natural edge strains are interpolated at the exceptional points, i.e.

$$\tilde{\gamma}_{\zeta s}(s) = G_1(s)\hat{\gamma}_{\zeta s}(s=\frac{1-\eta}{2}) + G_2(s)\hat{\gamma}_{\zeta s}(s=\frac{1}{2}) + G_3(s)\hat{\gamma}_{\zeta s}(s=\frac{1+\eta}{2}) \tag{16a}$$

$$\tilde{\gamma}_{\zeta t}(t) = G_1(t)\hat{\gamma}_{\zeta t}(t=\frac{1-\eta}{2}) + G_2(t)\hat{\gamma}_{\zeta t}(t=\frac{1}{2}) + G_3(t)\hat{\gamma}_{\zeta t}(t=\frac{1+\eta}{2}) \tag{16b}$$

$$\tilde{\gamma}_{\zeta r}(r) = G_1(r)\hat{\gamma}_{\zeta r}(r=\frac{1-\eta}{2}) + G_2(r)\hat{\gamma}_{\zeta r}(r=\frac{1}{2}) + G_3(r)\hat{\gamma}_{\zeta r}(r=\frac{1+\eta}{2}) \tag{16c}$$

where

$$\eta = \sqrt{5/3}\ ,\quad G_1(\xi) = \frac{(2\xi-1)(2\xi-1-\alpha)}{2\alpha^2}\ ,\quad G_2(\xi) = \frac{-(2\xi-1+\alpha)(2\xi-1-\alpha)}{\alpha^2}$$

$$G_3(\xi) = \frac{(2\xi-1)(2\xi-1+\alpha)}{2\alpha^2}$$

Their values at the pertinent element corners are then used to obtain the local Cartesian shear strains, i.e.

$$\begin{Bmatrix}\tilde{\gamma}_{zx1}\\ \tilde{\gamma}_{zy1}\end{Bmatrix} = \begin{bmatrix} z_{,\zeta}\,\partial_r x & z_{,\zeta}\,\partial_r y \\ z_{,\zeta}\,\partial_s x & z_{,\zeta}\,\partial_s y\end{bmatrix}^{-1}_{r=1,s=0} \begin{Bmatrix}\tilde{\gamma}_{\zeta r}(r=1)\\ \tilde{\gamma}_{\zeta s}(s=0)\end{Bmatrix} \qquad \text{at node 1} \tag{17a}$$

$$\begin{Bmatrix}\tilde{\gamma}_{zx4}\\ \tilde{\gamma}_{zy4}\end{Bmatrix} = \begin{bmatrix} z_{,\zeta}\,\partial_s x & z_{,\zeta}\,\partial_s y \\ z_{,\zeta}\,\partial_t x & z_{,\zeta}\,\partial_t y\end{bmatrix}^{-1}_{s=1,t=0} \begin{Bmatrix}\tilde{\gamma}_{\zeta s}(s=1)\\ \tilde{\gamma}_{\zeta t}(t=0)\end{Bmatrix} \qquad \text{at node 4} \tag{17b}$$

$$\begin{Bmatrix}\tilde{\gamma}_{zx7}\\ \tilde{\gamma}_{zy7}\end{Bmatrix} = \begin{bmatrix} z_{,\zeta}\,\partial_t x & z_{,\zeta}\,\partial_t y \\ z_{,\zeta}\,\partial_r x & z_{,\zeta}\,\partial_r y\end{bmatrix}^{-1}_{t=1,r=0} \begin{Bmatrix}\tilde{\gamma}_{\zeta t}(t=1)\\ \tilde{\gamma}_{\zeta r}(r=0)\end{Bmatrix} \qquad \text{at node 7} \tag{17c}$$

where

$$\partial_r x = \mathbf{e}_x^T(\partial_r \mathbf{X}_o)\ ,\ \partial_r y = \mathbf{e}_y^T(\partial_r \mathbf{X}_o)\ ,\ \partial_s x = \mathbf{e}_x^T(\partial_s \mathbf{X}_o)\ ,\ \partial_s y = \mathbf{e}_y^T(\partial_s \mathbf{X}_o)\ ,$$

$$\partial_t x = \mathbf{e}_x^T(\partial_t \mathbf{X}_o)\ ,\ \partial_t y = \mathbf{e}_y^T(\partial_t \mathbf{X}_o)\ ,\ z_{,\zeta} = \mathbf{e}_z^T \mathbf{X}_n$$

The six strains $\tilde{\gamma}_{\zeta r}(r=1)$, $\tilde{\gamma}_{\zeta s}(s=0)$, $\tilde{\gamma}_{\zeta s}(s=1)$, $\tilde{\gamma}_{\zeta t}(t=0)$, $\tilde{\gamma}_{\zeta t}(t=1)$ and $\tilde{\gamma}_{\zeta r}(r=0)$ form the set of six edge shear strains that results in the optimal constraint ratio.

The six non-edge shear strains are taken to be the ones directly evaluated at integration points *a*, *b* and *c*, see Fig.2a. Based on ($\tilde{\gamma}_{zx1}, \tilde{\gamma}_{zx4}, \tilde{\gamma}_{zx7}, \gamma_{zxa}, \gamma_{zxb}, \gamma_{zxc}$) and ($\tilde{\gamma}_{zy1}, \tilde{\gamma}_{zy4}, \tilde{\gamma}_{zy7}, \gamma_{zya}, \gamma_{zyb}, \gamma_{zyc}$), quadratic assumed γ_{zx} and γ_{zy} which are denoted as $\tilde{\gamma}_{zx}$ and $\tilde{\gamma}_{zy}$ can be obtained by interpolation. At integration stations *d*, *e* and *f*, it can be proved by straight forward but tedious algebra that $\tilde{\gamma}_{zx}$ and $\tilde{\gamma}_{zy}$ are given as :

$$\begin{Bmatrix}\tilde{\gamma}_{zxd}\\ \tilde{\gamma}_{zxe}\\ \tilde{\gamma}_{zxf}\end{Bmatrix} = \mathbf{A}_2^{-1}\begin{Bmatrix}\gamma_{zx1}\\ \gamma_{zx4}\\ \gamma_{zx7}\end{Bmatrix} - \mathbf{A}_2^{-1}\mathbf{A}_1\begin{Bmatrix}\gamma_{zxa}\\ \gamma_{zxb}\\ \gamma_{zxc}\end{Bmatrix}\ ,\quad \begin{Bmatrix}\tilde{\gamma}_{zyd}\\ \tilde{\gamma}_{zye}\\ \tilde{\gamma}_{zyf}\end{Bmatrix} = \mathbf{A}_2^{-1}\begin{Bmatrix}\gamma_{zy1}\\ \gamma_{zy4}\\ \gamma_{zy7}\end{Bmatrix} - \mathbf{A}_2^{-1}\mathbf{A}_1\begin{Bmatrix}\gamma_{zya}\\ \gamma_{zyb}\\ \gamma_{zyc}\end{Bmatrix} \tag{18a}$$

where

$$\mathbf{A}_1 = \begin{bmatrix} -c_1 & c_2 & -c_1 \\ -c_1 & -c_1 & c_2 \\ c_2 & -c_1 & -c_1 \end{bmatrix},\ \mathbf{A}_2 = \begin{bmatrix} c_3 & c_4 & c_4 \\ c_4 & c_3 & c_4 \\ c_4 & c_4 & c_3 \end{bmatrix},\ c_1 = 0.6385595874119381$$

$c_2 = 0.1263407264883946$, $c_3 = 1.8736592735116080$, $c_4 = 0.1385595874119366$

Symbolically, the assumed shear strains at integration station "*i*"can be expressed as :

$$\tilde{\boldsymbol{\gamma}}_i = \begin{Bmatrix} \tilde{\gamma}_{zxi} \\ \tilde{\gamma}_{zxi} \end{Bmatrix} = \tilde{\mathbf{B}}_{\gamma i}\mathbf{q} \tag{18b}$$

This completes the derivation of the assumed shear strains.

4. ASSUMED NATURAL MEMBRANE STRAINS

With γ_{zx} and γ_{zy} in Eqn.(13) replaced by $\tilde{\gamma}_{zx}$ and $\tilde{\gamma}_{zy}$, the resulting element still yields unsatisfactory accuracy in curved shell problems. This indicates that the membrane strains have to be refined. In this section, assumed natural strains will be employed. Different from the assumed strain method in the last section that involves the interpolation of local Cartesian shear strains, only the assumed natural membrane strains are interpolated in this section.

In quadrilateral assumed strain shell elements, the two normal and one shear natural membrane strains are interpolated (e.g., see Bathe & Dvorkin 1986; Huang & Hinton 1986; Jang & Pinsky 1987). To maintain cyclic symmetry in triangular elements, the following three natural normal membrane strains are interpolated (Sze & Zhu 1997b) :

$$\hat{\varepsilon}^m_{rr} = (\partial_r \mathbf{X}_o)^T(\partial_r \mathbf{U}_o),\ \hat{\varepsilon}^m_{ss} = (\partial_s \mathbf{X}_o)^T(\partial_s \mathbf{U}_o),\ \hat{\varepsilon}^m_{tt} = (\partial_t \mathbf{X}_o)^T(\partial_t \mathbf{U}_o) \tag{19}$$

In order that the element is rank sufficient, at least seventeen membrane strains have to be sampled. Naturally, six samples for each of $\hat{\varepsilon}^m_{rr}$, $\hat{\varepsilon}^m_{ss}$ and $\hat{\varepsilon}^m_{tt}$ are employed. For $\hat{\varepsilon}^m_{ss}$, they are chosen to be :

$$\hat{\varepsilon}^m_{ss}(s=\frac{1}{2}, t=0),\ \hat{\varepsilon}^m_{ss}(s=\frac{1\pm\alpha}{2}, t=0),\ \hat{\varepsilon}^m_{ss}(s=\frac{\sqrt{3}\pm 1}{3\sqrt{3}}, t=\frac{1}{3}),\ \hat{\varepsilon}^m_{ss}(s=\frac{1}{6}, t=\frac{2}{3}) \tag{20}$$

The first three sampling points at $t = 0$ are the same as that for $\tilde{\gamma}_{\zeta s}$. They are also optimal for a prescribed third order membrane strain field in a subparametric element and, due to their edge nature, are important to reduce the number of membrane constraints in the global level. The other two are the second order quadrature points of the $t = 1/3$ contour. Their mean is also optimal for a prescribed third order membrane strain field. The remaining one is the mid-point of the $t = 2/3$

contour. Based on these six $\widehat{\varepsilon}_{ss}^{m}$, a quadratic assumed $\widehat{\varepsilon}_{ss}^{m}$ can be obtained by interpolation. At the integration stations, $\widehat{\varepsilon}_{ss}^{m}$ are given as :

$$\begin{Bmatrix} \widetilde{\varepsilon}_{ssd}^{m} \\ \widetilde{\varepsilon}_{ssa}^{m} \\ \widetilde{\varepsilon}_{sse}^{m} \\ \widetilde{\varepsilon}_{ssb}^{m} \\ \widetilde{\varepsilon}_{ssf}^{m} \\ \widetilde{\varepsilon}_{ssc}^{m} \end{Bmatrix} = \mathbf{G} \begin{Bmatrix} \widehat{\varepsilon}_{ss}^{m}(s=(1-\alpha)/2, t=0) \\ \widehat{\varepsilon}_{ss}^{m}(s=1/2, t=0) \\ \widehat{\varepsilon}_{ss}^{m}(s=(1+\alpha)/2, t=0) \\ \widehat{\varepsilon}_{ss}^{m}(s=(\sqrt{3}+1)/(3\sqrt{3}), t=1/3) \\ \widehat{\varepsilon}_{ss}^{m}(s=1/6, t=2/3) \\ \widehat{\varepsilon}_{ss}^{m}(s=(\sqrt{3}-1)/(3\sqrt{3}), t=1/3) \end{Bmatrix} \tag{21a}$$

where matrix **G** in term of a FORTRAN-DATA statement is given in Appendix. The other two assumed natural membrane strains at the integration points are obtained by cyclic symmetry, i.e.

$$\begin{Bmatrix} \widetilde{\varepsilon}_{rrf}^{m} \\ \widetilde{\varepsilon}_{rrc}^{m} \\ \widetilde{\varepsilon}_{rrd}^{m} \\ \widetilde{\varepsilon}_{rra}^{m} \\ \widetilde{\varepsilon}_{rre}^{m} \\ \widetilde{\varepsilon}_{rrb}^{m} \end{Bmatrix} = \mathbf{G} \begin{Bmatrix} \widehat{\varepsilon}_{rr}^{m}(r=(1-\alpha)/2, s=0) \\ \widehat{\varepsilon}_{rr}^{m}(r=1/2, s=0) \\ \widehat{\varepsilon}_{rr}^{m}(r=(1+\alpha)/2, s=0) \\ \widehat{\varepsilon}_{rr}^{m}(r=(\sqrt{3}+1)/(3\sqrt{3}), s=1/3) \\ \widehat{\varepsilon}_{rr}^{m}(r=1/6, s=2/3) \\ \widehat{\varepsilon}_{rr}^{m}(r=(\sqrt{3}-1)/(3\sqrt{3}), s=1/3) \end{Bmatrix}, \quad \begin{Bmatrix} \widetilde{\varepsilon}_{tte}^{m} \\ \widetilde{\varepsilon}_{ttb}^{m} \\ \widetilde{\varepsilon}_{ttf}^{m} \\ \widetilde{\varepsilon}_{ttc}^{m} \\ \widetilde{\varepsilon}_{ttd}^{m} \\ \widetilde{\varepsilon}_{tta}^{m} \end{Bmatrix} = \mathbf{G} \begin{Bmatrix} \widehat{\varepsilon}_{tt}^{m}(t=(1-\alpha)/2, r=0) \\ \widehat{\varepsilon}_{tt}^{m}(t=1/2, r=0) \\ \widehat{\varepsilon}_{tt}^{m}(t=(1+\alpha)/2, r=0) \\ \widehat{\varepsilon}_{tt}^{m}(t=(\sqrt{3}+1)/(3\sqrt{3}), r=1/3) \\ \widehat{\varepsilon}_{tt}^{m}(t=1/6, r=2/3) \\ \widehat{\varepsilon}_{tt}^{m}(t=(\sqrt{3}-1)/(3\sqrt{3}), r=1/3) \end{Bmatrix} \tag{21b}$$

In analogous to Eqn.(8), the pertinent assumed local Cartesian membrane strains at integration station "*i*" can be expressed as :

$$\widetilde{\boldsymbol{\varepsilon}}_{i}^{m} = \begin{Bmatrix} \widetilde{\varepsilon}_{xxi}^{m} \\ \widetilde{\varepsilon}_{yyi}^{m} \\ 2\widetilde{\varepsilon}_{xyi}^{m} \end{Bmatrix} = \begin{bmatrix} (\partial_r x)_i^2 & (\partial_r y)_i^2 & (\partial_r x)_i(\partial_r y)_i \\ (\partial_s x)_i^2 & (\partial_s y)_i^2 & (\partial_s x)_i(\partial_s y)_i \\ (\partial_t x)_i^2 & (\partial_t y)_i^2 & (\partial_t x)_i(\partial_t y)_i \end{bmatrix}^{-1} \begin{Bmatrix} \widetilde{\varepsilon}_{rr}^{m} \\ \widetilde{\varepsilon}_{ss}^{m} \\ \widetilde{\varepsilon}_{tt}^{m} \end{Bmatrix}_i = \widetilde{\mathbf{B}}_{mi}\mathbf{q} \tag{22a}$$

where entries in the matrix have been defined in Eqn.(17) and $\widetilde{\mathbf{B}}_{mi}$ denotes symbolically the membrane strain-displacement matrix at the i-th integration station. This completes the derivation of the assumed membrane strain field.

5. SOFTENING THE MEMBRANE STIFFNESS BY HYBRID DESTABILIZING

A method to reduce the element stiffness associated with the membrane energy is the hybrid stress formulation (Pian 1964; Saleeb et al.1988; Sze 1993; Sze 1994; Pian 1995; Sze, Sim & Soh 1997).

By introducing the assumed stress into Eqn.(12), the following partial Hellinger-Reissner functional is formed :

$$\prod_{HR}^{e} = 2\int_0^1 \int_0^{1-t} (\frac{-1}{2} \boldsymbol{\sigma}_m^T \mathbf{C}_\varepsilon^{-1} \boldsymbol{\sigma}_m + \boldsymbol{\sigma}_m^T \boldsymbol{\varepsilon}_m + \zeta^2 \boldsymbol{\varepsilon}_b^T \mathbf{C}_\varepsilon \boldsymbol{\varepsilon}_b + \boldsymbol{\gamma}^T \mathbf{C}_\gamma \boldsymbol{\gamma}) J(\zeta = 0)\, ds\, dt \tag{23}$$

If the membrane stress is assumed to be :

$$\boldsymbol{\sigma}_m = \mathbf{P}_L \boldsymbol{\beta}_L \tag{24}$$

where

$\mathbf{P}_L = \left[\mathbf{I}_3 \quad s\mathbf{I}_3 \quad t\mathbf{I}_3 \quad (s^2 + 2st)\mathbf{I}_3 \quad (t^2 + 2st)\mathbf{I}_3\right]$ and $\boldsymbol{\beta}_L$ is vector of coefficients

the element stiffness matrix emerging from $\prod_{HR}^{e}$ is :

$$\mathbf{k} = \mathbf{G}_L^T \mathbf{H}_L^{-1} \mathbf{G}_L + \mathbf{k}_b + \mathbf{k}_\gamma \tag{25}$$

where

$$\mathbf{G}_L = 2\sum_{i=a}^{f} \mathbf{P}_{Li}^T \mathbf{B}_{mi} w_i J_i(\zeta = 0) \ , \ \mathbf{H}_L = 2\sum_{i=a}^{f} \mathbf{P}_{Li}^T \mathbf{C}_\varepsilon \mathbf{P}_{Li} w_i J_i(\zeta = 0)$$

This element suffers from the following spurious zero energy modes :

$$\begin{Bmatrix} u_s \\ u_t \end{Bmatrix} = \frac{1}{3} \begin{Bmatrix} 6t^3 - 6t^2 + 3t \\ 3s + 3t - 6t^2 - 12st - 12s^2 + 4t^3 + 6st^2 + 12s^2 t + 8s^3 \end{Bmatrix} \tag{26a}$$

and

$$\begin{Bmatrix} u_s \\ u_t \end{Bmatrix} = \frac{1}{3} \begin{Bmatrix} 3t + 3s - 6s^2 - 12st - 12t^2 + 4s^3 + 6ts^2 + 12t^2 s + 8t^3 \\ 6s^3 - 6s^2 + 3s \end{Bmatrix} \tag{26b}$$

The corresponding strain components are :

$$\frac{\partial u_{1s}}{\partial s} = 0 \ , \frac{\partial u_{1t}}{\partial t} = g \ , \frac{\partial u_{1s}}{\partial t} + \frac{\partial u_{1t}}{\partial s} = 2g \ , \frac{\partial u_{2s}}{\partial s} = g \ , \frac{\partial u_{2t}}{\partial t} = 0 \ , \frac{\partial u_{2s}}{\partial t} + \frac{\partial u_{2t}}{\partial s} = 2g \tag{27}$$

in which

$$g = 1 - 4s - 4t + 4s^2 + 4st + 4t^2 = 2r^2 + 2s^2 + 2t^2 - 1$$

These spurious zero energy modes have been checked to be incommutable and therefore do not plague any practical analysis. Moreover, it can be proved with the context of hybrid destabilization (Sze 1993; Sze et al. 1995) that

$$\mathbf{G}_L^T \mathbf{H}_L^{-1} \mathbf{G}_L = \mathbf{k}_m - \frac{1}{H_H} \mathbf{G}_H^T \mathbf{C}_\varepsilon \mathbf{G}_H \tag{28}$$

where

$$H_H = 2\sum_{i=a}^{f}(\frac{g_i}{J_i(\zeta=0)})^2 w_i J_i(\zeta=0)\ ,\ \mathbf{G}_H = 2\sum_{i=a}^{f}\frac{g_i}{J_i(\zeta=0)}\mathbf{B}_{mi} w_i J_i(\zeta=0)$$

Eqn.(28) is indeed a result of employing the following higher order membrane stress shape function matrix :

$$\mathbf{P}_H = \frac{g}{J(\zeta=0)}\mathbf{I}_3 \tag{29}$$

which are orthogonal to the $\mathbf{P}_L$ in the sense that

$$\int_0^1\int_0^{1-t}\mathbf{P}_H^T\mathbf{C}_\varepsilon\mathbf{P}_L\,ds\,dt = \mathbf{0}_{15\times3} \tag{30}$$

As (i) f is symmetric with respect to r, s, t and (ii) $\mathbf{I}_3$ is unbiased towards any of the membrane stress components, $\mathbf{G}_L^T\mathbf{H}_L^{-1}\mathbf{G}_L$ is invariant. The advantage of hybrid destabilization is that the large number of matrix operations involved in forming $\mathbf{G}_L^T\mathbf{H}_L^{-1}\mathbf{G}_L$ can be reduced.

6. NUMERICAL EXAMPLES

In this section, a number of popular benchmark tests are studied by five element models. Their stiffness matrix are given below :

model 1 : $\mathbf{k}_m + \mathbf{k}_b + \mathbf{k}_\gamma$ model 2 : $\mathbf{k}_m + \mathbf{k}_b + \tilde{\mathbf{k}}_\gamma$

model 3 : $\mathbf{k}_m + \mathbf{k}_b + \tilde{\mathbf{k}}_\gamma - \frac{1}{H_H}\mathbf{G}_H^T\mathbf{C}_\varepsilon\mathbf{G}_H$ model 4 : $\tilde{\mathbf{k}}_m + \mathbf{k}_b + \tilde{\mathbf{k}}_\gamma$

model 5 : $\tilde{\mathbf{k}}_m + \mathbf{k}_b + \tilde{\mathbf{k}}_\gamma - \frac{1}{H_H}\tilde{\mathbf{G}}_H^T\mathbf{C}_\varepsilon\tilde{\mathbf{G}}_H$

where

$$\tilde{\mathbf{k}}_m = 2\sum_{i=a}^{f}\tilde{\mathbf{B}}_{mi}^T\mathbf{C}_\varepsilon\tilde{\mathbf{B}}_{mi} w_i J_i(\zeta=0)\,,\ \tilde{\mathbf{k}}_\gamma = 2\sum_{i=a}^{f}\tilde{\mathbf{B}}_{\gamma i}^T\mathbf{C}_\gamma\tilde{\mathbf{B}}_{\gamma i} w_i J_i(\zeta=0)\,,\ \tilde{\mathbf{G}}_L = 2\sum_{i=a}^{f}\mathbf{P}_{Li}^T\tilde{\mathbf{B}}_{mi} w_i J_i(\zeta=0)$$

The remaining matrices have been defined in Eqn.(13). In particular, model 5 employs both assumed membrane strains and destabilization.

Unless specified otherwise, the material Poisson's ratio is taken to be 0.3 and the model predictions are normalized by the reference solutions presented in (MacNeal & Harder 1985).

6.1 Patch Test All the models pass the constant bending stress, membrane stress and transverse shear stress patch tests prescribed by MacNeal & Harder (1985).

6.2 Zero Energy Modes The only zero energy modes of models 1, 2 and 4 are the six rigid body modes. With a flat plate geometry, models 3 and 5 have two extra zero energy modes, see Fig.3. However, with a curved shell geometry, the two extra zero energy modes disappears as these modes also contribute to the bending and transverse shear energies.

6.3 Shear Locking Test The fully clamped ($w = \theta_x = \theta_y = 0$ at all edges) square plate of side length L and thickness h is subjected to a central point load. Owing to symmetry, only one quarter of structure is modelled, see Fig.4a. The central deflections predicted by 1×1 and 2×2 meshes for different L to h ratios are normalized by Timoshenko & Woinowsky-Krieger (1970)'s thin plate solutions and listed in Table 1. All models suffer no severe shear locking but the ones using the assumed shear strains are much more accurate.

Table 1. Normalized central deflections for fully clamped square plate subjected to central point load, see Fig.4a

	mesh	L/h = 100	L/h = 1 000	L/h = 100 000
model 1	1 x 1	0.672	0.595	0.594
	2 x 2	0.936	0.876	0.874
models 2, 3, 4 & 5	1 x 1	1.019	1.009	1.009
	2 x 2	0.996	0.992	0.992

6.4 Fully Clamped Square Plates A fully clamped square plate of L to h fixed at 1000 is considered. A quadrant of the plate is modelled as shown in Fig.4a. The plate is subjected to central point load and uniform pressure. The deflections and bending moments at the centre of the plate are normalized by Timoshenko & Woinowsky-Krieger (1970)'s thin plat solutions and listed in Table 2. The models using the assumed shear strains are more accurate.

Table 2. Normalized central deflections and bending moments for fully clamped square plate, see Fig.4a

	mesh	central deflection under point load	central deflection under uniform pressure	central bending moment under uniform pressure
model 1	2 × 2	0.876	0.895	1.107
	3 × 3	0.956	0.971	1.121
	4 × 4	0.979	0.991	1.067
models 2, 3, 4 & 5	2 × 2	0.992	1.006	0.947
	3 × 3	0.998	1.004	0.971
	4 × 4	1.000	1.004	1.003

6.5 Fully Clamped Circular Plates A fully clamped circular plate of diameter to thickness ratio equal to 1000 is considered. A quadrant of the plate is modelled by 2, 6 and 12 elements, see Fig.4b. The plate is subjected to central point load and uniform pressure. The predicted central deflections and bending moments are normalized by Timoshenko & Woinowsky-Krieger (1970)'s

thin plate solutions and listed in Table 3. Again, the models using the assumed shear strains are more accurate.

Table 3. Normalized central deflections and bending moment for fully clamped circular plate, see Fig.4b

	number of elements	central deflection under point load	central deflection under uniform pressure	central bending moment under uniform pressure
model 1	2	0.038	0.135	1.310
	6	0.857	0.820	0.428
	12	0.974	0.966	0.916
models 2,	2	0.989	1.018	0.725
3, 4 & 5	6	0.991	1.003	0.983
	12	0.998	1.001	0.989

6.6 Curved Beam The curved beam is portrayed in Fig.5a. The beam is of unit thickness and fully clamped at the supported end. At the free end, in-plane and out-of-plane forces are applied. The normalized end deflections along the loading directions are tabulated in Table 4. It can be seen that the destabilization renders model 3 and model 5 more flexible than the others under the inplane loading. As the beam is quite thick, shear locking is not triggered and thus all elements are of the same accuracy for the out-of-plane loading.

Table 4. Normalized tip deflections for curved beam, see Fig.5a

	model 1	model 2	model 3	model 4	model 5
inplane	1.012	1.012	1.032	1.012	1.043
out-of-plane	0.991	0.988	0.988	0.988	0.988

6.7 Twisted Beam Problem Fig.5b depicts a 90^o pre-twisted beam. At its clamped end, all d.o.f s are restrained. End forces are applied to the free end. This is often considered to be a good test for membrane locking (Belytschko et al. 1989). After normalized by the reference solutions (Belytschko et al. 1989), the end deflections for two different thickness are given in Table 5. When thickness equals 0.32, all models yield very good accuracy. However, when the thickness is reduced to 0.0032, model 5 out-performs the others.

Table 5. Normalized end deflections for twisted beam, see Fig.5b

	4 × 10 nodes per side				4 × 19 nodes per side			
	inplane loading		out-of-plane loading		inplane loading		out-of-plane loading	
	0.32	0.0032	0.32	0.0032	0.32	0.0032	0.32	0.0032
model 1	0.994	0.927	0.996	0.886	0.997	0.973	0.999	0.968
model 2	0.996	0.927	0.997	0.880	0.998	0.972	0.999	0.966
model 3		0.948		0.904	0.998	0.981	1.002	0.974
model 4	0.996	0.937	0.999	0.922	0.998	0.986	1.000	0.992
model 5	0.997	0.982	1.008	0.954	0.998	1.000	1.003	0.996

6.8 Pinched Spherical Shell A spherical shell is pinched by two diametrically opposite forces, see Fig.6a. This is the only one doubly curved problem found in the paper by Lee et al (1985) in which

the shell is modelled mainly by quadrilateral macro-elements. Starting from Z-axis, the segmental angles $\Delta\phi$'s are 2^o, 3^o, 3^o, 8^o, 12^o, 17^o, 22.5^o and 22.5^o. Downward deflections at the upper pole are normalized by Koiter (1963)'s thin shell solutions and listed in Table 6 for different radius to thickness (R/t) ratios. When R/t equals 50, all finite element predictions are about 10% larger than the reference solutions. It is due to the ignorance of shear deformation in Koiter's solutions. Even model 1 performs very well when macro-quadrilateral elements are employed. Unfortunately, they do not possess the advantage of triangular elements in automatic mesh generation and refinement.

Table 6. Normalized downward deflections for spherical shell, see Fig.6a

R/t	model 1	model 2	model 3	model 4	model 5	Lee et al [4]
50	1.102	1.097	1.098	1.098	1.100	1.103
500	1.003	1.003	1.005	1.003	1.005	1.022
1000	0.999	0.986	0.990	0.984	0.989	1.014

6.9 Hemispherical Shell This is a popular benchmark problem in which a hemispherical shell with a 18^o hole cut-out is subjected to anti-symmetric point loads at its bottom. By taking advantage of the symmetry, only one quarter of the shell is modelled, see Fig.6b. Radial deflections for different mesh densities at the points of loading are normalized and listed in Table 6. Model 5 which employs both assumed membrane strains and destabilization are most accurate.

Table 7. Normalized radial deflections for hemispherical shell, see Fig.6b

nodes/side	7	13	19	25	37	49
model 1	0.090	0.715	0.942	0.981	0.994	0.996
model 2	0.283	0.779	0.952	0.986	0.997	0.997
model 3	0.418	0.887	0.984	0.997	0.999	0.998
model 4	0.872	0.962	0.990	0.996	0.998	0.998
model 5	0.974	0.997	1.002	1.002	0.999	0.998

6.10 Scordelis-Lo Roof This problem is depicted in Fig.7a. The shell is loaded by its own weight specified as g unit force per unit mid-surface area. The roof is mounted on two rigid end diaphragms over which $u = w = \theta_y$. The two longitudinal edges remain free-hanging. Only a quarter of the roof is analyzed due to symmetry. The vertical deflections at point A are computed, normalized and listed in Table 7. All models yield accurate predictions in this problem.

Table 8. Normalized tip deflections for the Scordelis-Lo roof, see Fig.7a

nodes/side	7	10	13	16	19	25
model 1	0.944	0.991	0.995	0.996	0.997	0.997
model 2	0.954	0.994	0.997	0.997	0.997	0.997
model 3	1.029	1.005	1.000	0.998	0.998	0.997
model 4	0.995	0.999	0.998	0.998	0.998	0.997
model 5	1.030	1.005	1.000	0.998	0.998	0.997

6.11 Pinched cylinder The thin cylinder depicted in Fig.7b is subjected to diametrically opposite point loads. The cylinder is supported by two rigid end diaphragms over which $u = w = \theta_y$. Owing

to symmetry, one octant of the cylinder is modelled. The predicted deflections under the point load are normalized as in Table 9. The destabilized elements (models 3 and 5) are most accurate.

Table 9. Normalized tip deflections for a pinched cylinder, see Fig.7b

nodes/side	7	10	13	16	19	25
model 1	0.382	0.587	0.757	0.859	0.916	0.969
model 2	0.535	0.677	0.831	0.918	0.959	0.990
model 3	0.745	0.859	0.928	0.964	0.981	0.997
model 4	0.617	0.782	0.900	0.958	0.976	0.998
model 5	0.767	0.864	0.938	0.975	0.989	1.000

7. CLOSURE

In this paper, the assumed strain method in which the local Cartesian strains are interpolated is employed to reduce the shear stiffness of the ten-node element. Two measures are devised for refining the membrane stiffness. The first one is to employ the assumed natural strain method in which three different natural normal membrane strain components are interpolated. This stands a sharp difference from the assumed natural strain quadrilaterals where two normal and one shear membrane strains are interpolated. The second measure is the hybrid destabilization that softens the membrane stiffness by inducing two incommutable spurious zero energy modes. Popular numerical tests are exercised and the results reveal the efficacy of the proposed devices on improving the ten-node element.

Acknowledgment - The financial support of *Hong Kong Research Grant Council* is gratefully acknowledged.

REFERENCES

Ahmad, S.; Irons, B.M.; Zienkiewicz, O.C.(1970): Analysis of thick and thin shell structures by curved finite elements. Inter.J.Numer.Methods Engrg., **42**, 419-451

Basar, Y., Ding, Y. (1996) : Finite element analysis of hyperelastic thin shells with large strains. Computational Mechanics, **18**, 200-214

Brank, B.; Peric, D.; Damjanic, F.B. (1995) : On implementation of a nonlinear four node shell finite element for thin multilayered elastic shells, Computational Mechanics, **16**, 341-359

Bathe, K.-J.; Dvorkin, E.N.(1986): A formulation of general shell elements - the use of mixed interpolation of tensorial components, Inter.J.Numer.Methods Engrg., **22**, 697-722

Bathe, K.-J.; Bucalem, M.L; Brezzi, F.(1990): Displacement and stress convergence of our MITC plate bending elements. Engineering Computations, **7**, 291-302

Bathe, K.-J.(1996): Finite Element Procedures, Prentice Hall, New Jersey

Belytschko, T.; Wong, B.K.; Stolarski, H.(1989): Assumed strain stabilization procedure for the 9-node Lagrange shell element. Inter.J.Numer.Methods.Engrg., **28**, 385-414

Cook, R.D.; Malkus, D.S.; Plesha, M.E.(1989): Concepts and Applications of Finite Element Analysis, 3rd edn., John Wiley & Sons, New York

Flores, F.G.; Oñate, E.; Zarate, R. (1996) : New assumed strain triangles for nonlinear shell analysis, Computational Mechanics, **17**, 107-114

Fung, Y.C.(1965): Foundation of Solid Mechanics, Prentice-Hall, Englewood Cliffs, New Jersey

Huang, H.C.; Hinton, E.(1986): A new nine node degenerated shell element with enhanced membrane and shear interpolation. Inter.J.Numer.Methods Engrg., **22**, 73-92

Hughes, T.J.R.(1987): The Finite Element Method - Linear Static and Dynamic Finite Element Analysis. Prentice-Hall, New Jersey

Jang, J.-H.; Pinsky, P.M.(1987): An assumed covariant strain based 9-node shell element. Inter.J.Numer. Methods Engrg., **24**, 2389-2411

Koiter, W.T.(1963): A spherical shell under point loads at its poles. Progress in Appl.Mech., The Prager Anniversary Volume, pp.155-169, MacMillan

Lee, S.W.; Dai, C.C.; Yeom, C.H.(1985): A triangular finite element for thin plates and shells.Inter.J. Numer. Methods Engrg., **21**, 1813-1831

MacNeal, R.H.; Harder, R.L.(1985): A proposed standard set of problems to test finite element accuracy. Finite Elements in Analysis & Design, **1**, 3-20

Militello, C.; Felippa, C.A.(1991): The first ANDES elements : 9-dof plate bending triangles. Computer Methods Appl.Mech.Engrg.**, 93**, 217-246

Pian, T.H.H.(1964): Derivation of element stiffness matrices by assumed stress distributions. AIAA J., **2**, 1333-1336

Pian, T.H.H.(1995): State-of-the-art Development of Hybrid/Mixed Finite Element Method. Finite Elements in Analysis & Design, **21**, 5-20

Saleeb, A.F.; Chang, T.Y.; Yingyeunyong, S.(1988): A mixed formulation of C^0-linear triangular plate/ shell element - the role of edge shear constraints. Inter.J.Numer.Methods Engrg., **26**, 1101-1128

Sze, K.Y.(1993): A novel approach for devising higher order hybrid elements. Inter.J.Numerical Methods Engrg., **36**, 3303-3316

Sze, K.Y.(1994): An explicit hybrid-stabilized 9-node Lagrangian shell element. Computer Methods Applied Mechanics & Engrg., **117**, 361-379

Sze, K.Y.; Fan, H.; Chow, C.L.(1995): Elimination of spurious kinematic and pressure modes in biquadratic plane element. Inter.J.Numerical Methods Engrg., **38**, 3911-3932

Sze, K.Y.; Zhu, D.; Chen, D.-P.(1997): Quadratic Triangular C^0 Plate Bending Element. Inter.J.Numer.Methods Engrg., **40**, 937-951

Sze, K.Y.; Sim, Y.S.; Soh, A.K.(1997): A hybrid stress quadrilateral shell element with full rotational d.o.f.s. Inter.J.Numerical Methods Engrg., **40**, 1785-1800

Sze, K.Y.; Zhu, D.(1997a): A simple assumed strain method for enhancing the accuracy of the cubic triangular C^0 plate bending element. Finite Elements in Analysis & Design, accepted

Sze, K.Y.; Zhu, D.(1997b): A quadratic assumed natural strain curved triangular shell element. submitted to Computer Methods in Applied Mathematics & Engineering

Timoshenko, S.P.; Woinowsky-Krieger, S. 1970): Theory of Plates and Shells, 2nd Edn., McGraw-Hill, New York

Zienkiewicz, O.C.; Taylor, R.L (1989): The Finite Element Method, 4th Edn., McGraw-Hill, London

APPENDIX

Entries in G, see Eqn.(21), are given in the following FORTRAN-DATA statement :

```
      data G/  .7630831301561593d0,  -.1947933738919082d0,  .0573551959053217d0,
     &        -.0218462712658506d0,  -.0996264073011143d0,  .4958277263973922d0,
     &        -.0724588994900007d0,   .711042398640394d0,  -.0724588994900007d0,
     &         .2717208730875027d0,  -.1095663458353977d0,  .2717208730875027d0,
     &         .0573551959053238d0,  -.1947933738919129d0,  .7630831301561638d0,
     &         .4958277263973927d0,  -.0996264073011143d0,  -.0218462712658511d0,
     &         .0611780290812201d0,  -.0810747191220701d0,  -.0919562646049737d0,
     &        1.030076003496703d0,    .2259925181020718d0,  -.1442155669529514d0,
     &         .1472098905965136d0,   .0323459490732081d0,   .1472098905965114d0,
     &        -.5520370897369184d0,  1.777308449207609d0,   -.5520370897369236d0,
     &        -.0919562646049732d0,  -.0810747191220704d0,   .0611780290812206d0,
     &        -.1442155669529504d0,   .2259925181020718d0,  1.030076003496702d0  /
```

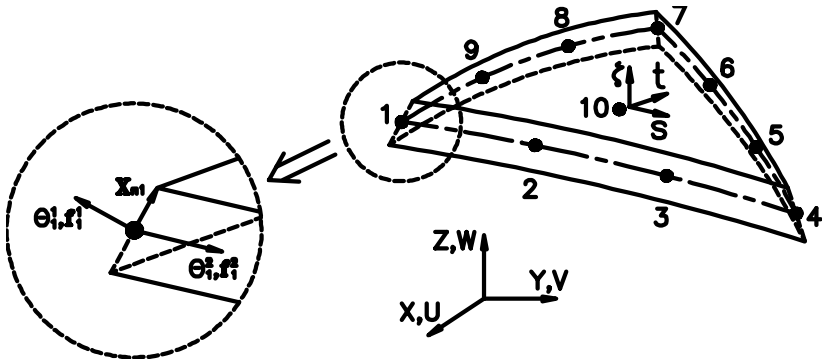

Figure 1. Description of a ten-node degenerated shell element

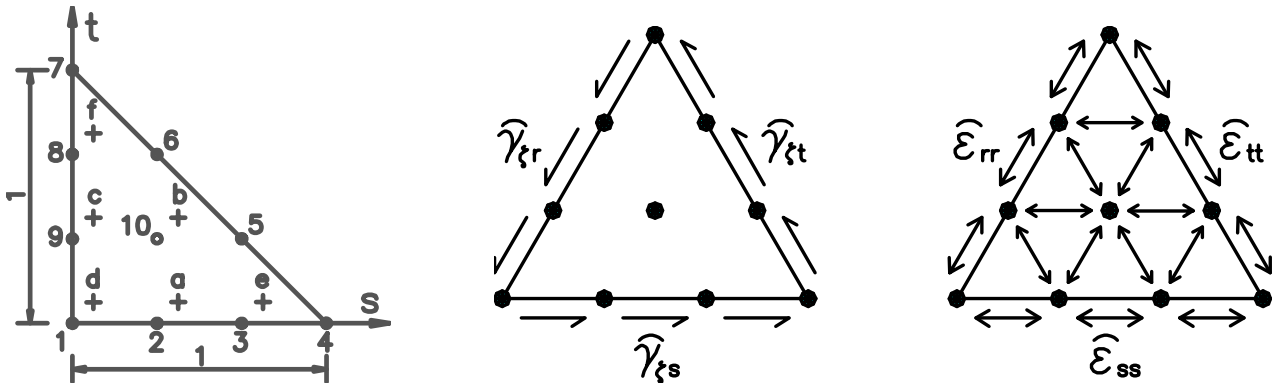

(a) (b) (c)

Figure 2. (a) Designation for integration stations; (b) Sampled natural shear strains; (c) sampled natural membrane strains

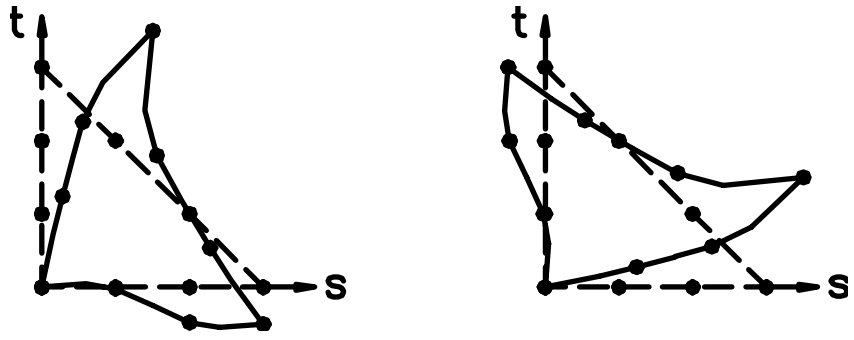

Figure 3. Extra zero energy modes for destabilized elements; chained lines depict the undeformed element

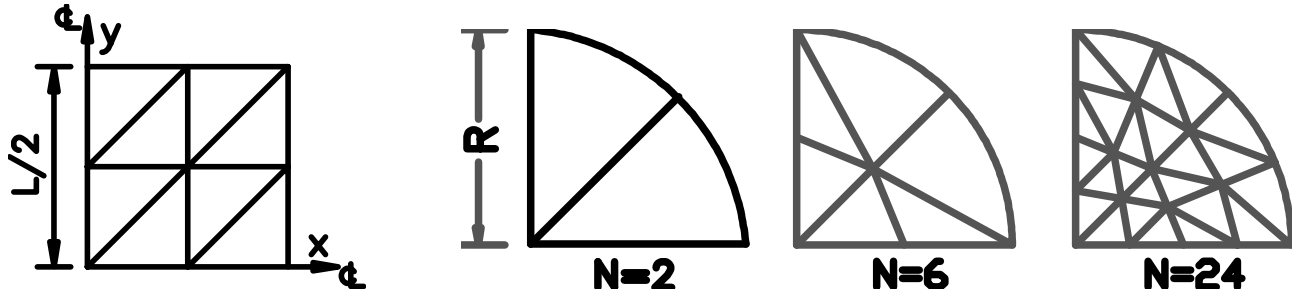

(a) (b)

Figure 4. (a) A quadrant of a square plate modelled by the 2×2 mesh;
(b) A quadrant of a circular plate modelled by two, six and twelve elements

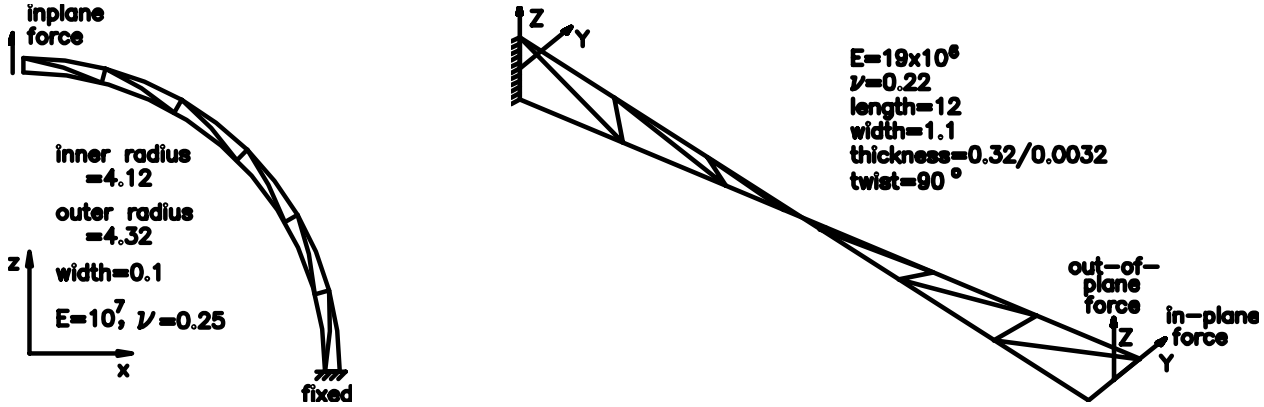

Figure 5. (a) Curved beam problem;
(b) Twisted beam problem modelled by 5×25 nodes/side

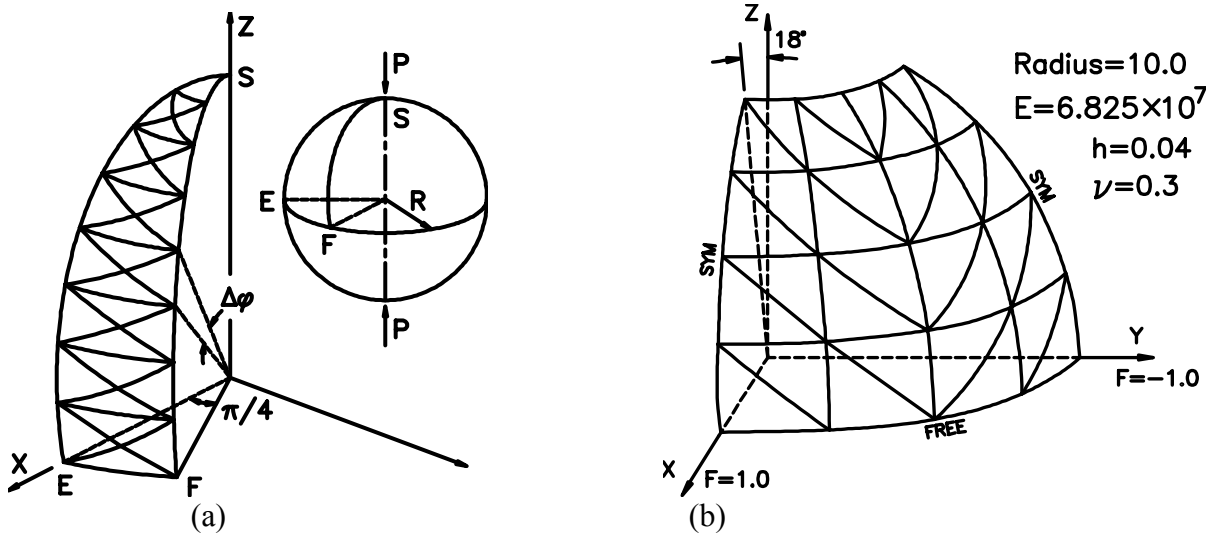

(a) (b)

Figure 6. (a) Pinched spherical shell; (b) Hemispherical shell modelled by thirteen nodes/side

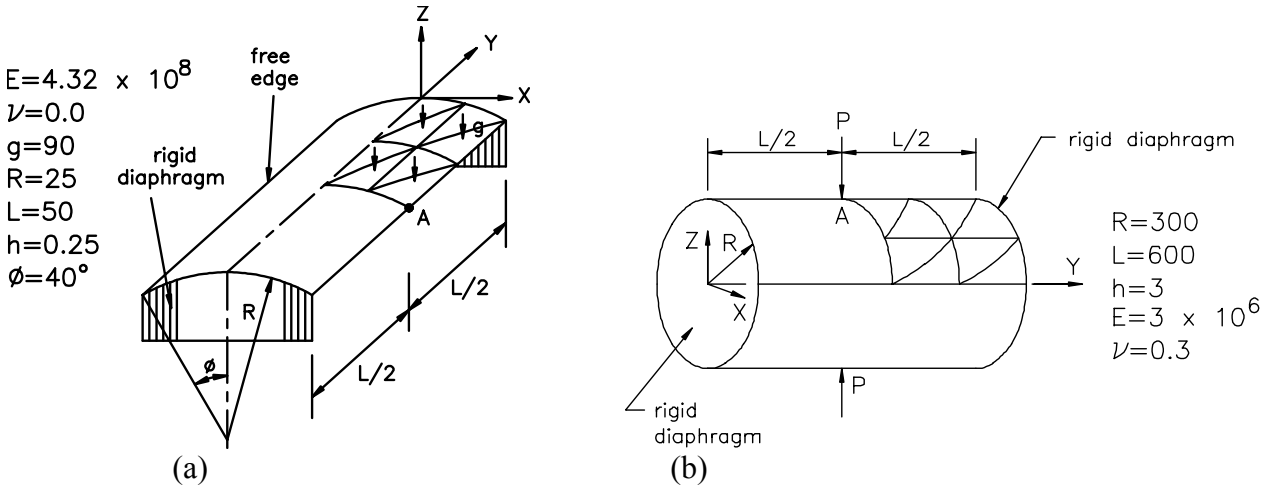

Figure 7. (a) Scordelis-Lo roof modelled by seven nodes/side;
(b) Pinched cylindrical shell modelled seven nodes/side